The final publication is available at:
http://link.springer.com/article/10.1007%2Fs00269-012-0493-0

Physics and Chemistry of Minerals
May 2012, Volume 39, Issue 5, pp 385-397
10.1007/s00269-012-0493-0

On the thermo-elastic behaviour of clintonite up to 10 GPa and 1000 °C

G. Diego Gatta, Marco Merlini, Hanns-Peter Liermann, André Rothkirch, Mauro Gemmi, Alessandro Pavese

Running title: H*P*-H*T* behavior of clintonite

Corresponding author: G. Diego GATTA

Dip. Scienze della Terra
Universita' degli Studi di Milano
Via Botticelli, 23
I-20133 Milano, Italy
Tel. +39 02 503 15607
Fax +39 02 503 15597
E-Mail: diego.gatta@unimi.it

On the thermo-elastic behaviour of clintonite up to 10 GPa and 1000 °C

[1,2]G. Diego Gatta, [1]Marco Merlini, [3]Hanns-Peter Liermann, [3]André Rothkirch, [4]Mauro Gemmi, [1,2]Alessandro Pavese

[1]Dipartimento di Scienze della Terra, Università degli Studi di Milano, Via Botticelli 23, I-20133 Milano, Italy

[2]CNR-Istituto per la Dinamica dei Processi Ambientali, Milano, Italy

[3] DESY, HASYLAB, PETRA III, Notkestr. 85, D-22607 Hamburg, Germany

[4]NEST, Istituto Italiano di Tecnologia, Piazza San Silvestro 12,I- 56127 Pisa, Italy

Abstract

The thermo-elastic behaviour of a natural clintonite-1*M*[with composition: $Ca_{1.01}(Mg_{2.29}Al_{0.59}Fe_{0.12})_{\Sigma 3.00}(Si_{1.20}Al_{2.80})_{\Sigma 4.00}O_{10}(OH)_2$] has been investigated up to 10 GPa (at room temperature) and up to 960 °C (at room pressure) by means of in-situ synchrotron single-crystal and powder diffraction, respectively. No evidence of phase transition has been observed within the pressure- and temperature-range investigated. *P*-*V* data fitted with an isothermal third-order Birch-Murnaghan Equation of State (BM-EoS) give: V_0= 457.1(2)Å^3, K_{T0}= 76(3)GPa and *K'*= 10.6(15). The evolution of the "Eulerian finite strain" *vs* "normalized stress" shows a linear positive trend. The linear regression yields *Fe*(0) = 76(3) GPa as intercept value, and the slope of the regression line leads to a *K'* value of 10.6(8). The evolution of the lattice parameters with pressure is significantly anisotropic [$\beta(a) = 1/3K_{T0}(a) = 0.0023(1)$ GPa^{-1}; $\beta(b) = 1/3K_{T0}(b) = 0.0018(1)$ GPa^{-1}; $\beta(c) = 1/K_{T0}(c) = 0.0072(3)$ GPa^{-1}]. The β-angle increases in response to the applied *P*, with: $\beta_P = \beta_0 + 0.033(4)P$ (*P* in GPa). The structure refinements of clintonite up to 10.1 GPa show that under hydrostatic pressure the structure rearranges by compressing mainly isotropically the inter-layer Ca-polyhedron. The bulk-modulus of the Ca-polyhedron, described using a second order-BM-EoS, is K_{T0}(Ca-polyhedron) = 41(2) GPa. The compression of the bond distances between calcium and the basal oxygens of the tetrahedral sheet leads, in turn, to an increase of the ditrigonal distortion of the tetrahedral ring, with $\partial\alpha/\partial P \approx 0.1$ °/GPa within the *P*-range investigated. The Mg-rich octahedra appear to compress in response of the applied pressure, whereas the tetrahedron appears to behave as a rigid unit. The evolution of axial and volume thermal expansion coefficient α with temperature was described by the polynomial $\alpha(T) = \alpha_0 + \alpha_1 T^{1/2}$. The refined parameters for clintonite are: $\alpha_0 = 2.78(4)\cdot10^{-5}$ °C^{-1} and $\alpha_1 = -4.4(6)\cdot10^{-5}$ °C$^{1/2}$for the unit-cell volume, $\alpha_0(a) = 1.01(2)\cdot10^{-5}$ °C^{-1} and $\alpha_1(a) = -1.8(3)\cdot10^{-5}$ °C$^{1/2}$ for the *a*-axis, $\alpha_0(b) = 1.07(1)\cdot10^{-5}$ °C^{-1} and $\alpha_1(b) = -2.3(2)\cdot10^{-5}$ °C$^{1/2}$ for the *b*-axis, $\alpha_0(c) = 0.64(2)\cdot10^{-5}$ °C^{-1} and $\alpha_1(c) = -7.3(30)\cdot10^{-6}$ °C$^{1/2}$for the *c*-axis. The β angle appears to be almost constant within the given *T*-range. No structure collapsing in response to the *T*-induced

dehydroxylation was found up to 960 °C. The H*P*- and H*T*-data of this study show that in clintonite the most and the less expandable directions do not correspond to the most and the less compressible directions, respectively. A comparison between the thermo-elastic parameters of clintonite and those of *true micas* was carried out.

Keywords: clintonite, micas, high-temperature, high-pressure, synchrotron diffraction, thermal expansion, compressibility.

Introduction

Clintonite (often called xanthophyllite, Forman et al. 1967, Guggenheim 1984) is a rare trioctahedral *brittle mica* with ideal composition $Ca(Mg_2Al)(Al_3Si)O_{10}(OH)_2$, which forms as a result of thermal metamorphism of Ca- and Al-rich, Si-poor rocks. It was found in chlorite schists, in metasomatically altered limestones, or in siliceous skarns in proximity to the near-contact metamorphic zones (*e.g.* Warnet and Luth 1973; Raymond 1976; Rice 1979; Tracy 1979; Ulmer 1982; Sugaki et al. 2000; Woodford et al. 2001; Houzar and Novák 2006). A series of studies have been devoted to the crystal chemistry, phase stability of clintonite and petrological implications (*e.g.* Kushiro and Yoder 1964; Olesch 1975; Olesch and Seifert 1976; Annersten and Olesch 1978; Ulmer 1982). From a crystallochemical point of view, an interesting feature of clintonite is in the violation of the Loewenstein's aluminum avoidance rule (Loewenstein 1954), due to the Al/Si (a.p.f.u.) >2. In contrast, in the parent *brittle mica* margarite (ideally $CaAl_2(Al_2Si_2)O_{10}(OH)_2$), equal amounts of Si and Al lead to an almost complete (Si,Al)-ordering in the tetrahedral sites (*e.g.* Farmer and Velde 1973; Guggenheim and Bailey 1975, 1978; Joswig et al. 1983).

Following the first experiments aimed at describing the crystal structure (Sanero 1940; Takéuchi 1966; Takéuchi and Sadanaga 1959; Fig. 1), a single-crystal neutron diffraction study of a clintonite-1*M* from Lago della Vacca, Adamello, Italy, [with composition: $(Ca_{1.00}Na_{0.007})(Mg_{2.29}Al_{0.70}Fe^{2+}_{0.05}Ti_{0.006})(Al_{2.69}Si_{1.20}Fe^{3+}_{0.11})O_{10}(OH)_2$] by Joswig et al. (1986), along with a Mössbauer experiment, confirmed: 1) the disordered (Si,Al)-distribution in the tetrahedral sheet, 2) provided a clear picture of the H position and of the H-bonding scheme in this phyllosilicate, and 3) showed that the Fe^{2+} is incorporated into the octahedral site, whereas the Fe^{3+}, although in competition with an excess of Al^{3+}, is almost completely at the tetrahedral site. Additional comparative studies of clintonites-1*M* from different localities were reported by MacKinney et al. (1988) and Alietti et al. (1997). In the latter, homologies and differences between clintonite and the closely related Al-rich phlogopite were highlighted. The crystallochemical data reported so far showed that natural clintonites appear to have only minor substitutions of elements

outside the ideal composition (*i.e.* Ca, Mg, Al, Si). Among those, the most important substituent is Fe.

To the best of our knowledge, no experiment has so far been devoted to the high pressure (H*P*) and high temperature (H*T*) behavior of *brittle micas*, and so no thermo-elastic data are available for this class of materials. In the framework of our comparative studies of phase stability, elastic behavior and *P/T*-induced structure evolution of phyllosilicates (*e.g.* Pavese et al. 2003, 2007; Gemmi et al. 2008; Gatta et al. 2009, 2010, 2011) it is the aim of this investigation to address the thermo-elastic behavior of a natural clintonite by in-situ H*T* and H*P* synchrotron diffraction. A comparison between the thermo-elastic parameters of clintonite and those of *true micas* is carried out.

Experimental methods

A natural clintonite from the methamorphic complex of Lago della Vacca, Adamello, Italy, was used in this study. Clintonite crystals occur in marly dolomites localized in the contact zone between gabbroic cumulates and the intermediate intrusions of the Re di Castello Pluton at the southern border of the Tertiary, calcalkaline Adamello Massif. The following mineral assemblages formed as a result of a high temperature contact metamorphism: monticellite-forsterite-clintonite (near the contact with the gabbroic cumulates) and forsterite-diopside-clintonite (away from the contact) (Ulmer 1982).

Electron microprobe analysis of clintonite in wavelength dispersive mode (EMPA-WDS) was performed on several crystals (optically free of defect or zoning) using a ARL-SEMQ microprobe. Major and minor elements were determined at 15 kV accelerating voltage and 10 nA beam current with a counting time of 20 seconds. The standards employed were: albite (Al, Si, Na), celsian (Ba), microcline (K), anorthite (Ca), fayalite (Fe), and forsterite (Mg). The crystals appear to be chemically homogeneous and the chemical formula (obtained by averaging 30 points analyses) is: $Ca_{1.01}(Mg_{2.29}Al_{0.59}Fe_{0.12})_{\Sigma 3.00}(Si_{1.20}Al_{2.80})_{\Sigma 4.00}O_{10}(OH)_2$.

The quality of a large number of crystals (about 40) were examined with a Xcalibur – Oxford Diffraction diffractometer equipped with a CCD, in order to find a crystal of clintonite with a regular stacking sequence suitable for the high pressure experiment. Only a few small crystals (< 60 x 60 x 15 μm) showed no diffuse streaks parallel to c^* for reflections with $k \neq 3n$, suggesting a complete stacking ordering (Nespolo and Ferraris 2001; Nespolo and Ďurovič 2002). The absence of $h + k \neq 2n$ reflections and the intensity distribution along rows [13*l*] and [02*l*] confirmed the *C*-centered lattice and the 1*M* polytype (Bailey 1988) for the clintonite crystals investigated here. H*P*-

synchrotron X-ray single-crystal diffraction experiments were performed at beamline P02.2 (Extreme Conditions Beamline) at DESY/PETRA III, using X-rays with an energy of 42.7 keV (0.29036 Å wavelength) and a focusing spot of ~ 2.0 (H) x 1.8 (V) μm² originating from a 320 mm KB mirror system. Sample detector distance of 401.34 mm was calibrated using a CeO_2 standard (NIST 674a). A single crystal of clintonite (~ 50 x 50 x 15 μm) was loaded in a Boehler Almax type diamond anvil cell (DAC) with a 70° opening and equipped with diamonds of 400 μm culets size. A 250 μm thick rhenium gasket was indented to 40 μm and drilled with 196 μm hole that contained the sample, a mixture of methanol:ethanol = 4:1 as pressure transmitting medium (Angel et al. 2007) and some calibrated ruby spheres for pressure determination (Mao et al. 1986). Pressure was increased mechanically through the Boehler Almax gear device and measured with the offline ruby/alignment system located in the laser lab of the Extreme Condition Science Infrastructure (ECSI) at PETRA III. Diffraction images were acquired on a MAR345 online image plate using an in house script for collecting step-scan diffraction images. MAR345 image files were collected with a pixel resolution of 150 x 150 microns to reduce data collection time. After collection, the images were converted with an in house software script to conform to the standard format of the program CrysAlis (Oxford Diffraction 2010).

The diffraction data were first collected at ambient pressure, with the crystal in the DAC and without any *P*-medium (Table 1). A pure ω-scan ($-30 \leq \omega \leq +30°$), with a step size of 1° and a time of 1 s/frame was used to maximize the accessible reciprocal space portion. Intensities were integrated and corrected for Lorentz-polarization (Lp) effects, using the CrysAlis package (Oxford Diffraction 2010). The reflection conditions were consistent with those of the space group *C*2/*m* according to previous experimental findings (e.g. Alietti et al. 1997). The diffraction pattern showed a substantial absence of stacking disorder. The isotropic structural refinement was conducted using the SHELX-97 software (Sheldrick 1997), starting from the atomic coordinates of Alietti et al. (1997) for a clintonite-1*M* and adopting a H-free structural model. Neutral atomic scattering factors of Ca, Mg, Al, Si and O from the International Tables for Crystallography (Wilson and Prince 1999) were used. In particular: (1) the X-ray scattering curve of calcium yielded an interlayer site fully occupied (Table 2); (2) a Mg/Al mixed scattering curve (*i.e.* 80% Mg and 20% Al) was used to model the octahedral M1 and M2 sites, and (3) an Al-Si mixed scattering curve (*i.e.* 70% Al and 30% Si) was used to model the tetrahedral site (*i.e.* T, Table 2), though this did not improve the figures of merit of the refinements with respect to those obtained by the X-ray scattering curve of Mg only at the M1 and M2 sites and Al only at the T site, respectively. When convergence was achieved, no residual peak larger than $-0.35/+0.36 e^-/Å^3$ was present in the final difference-Fourier

synthesis (Table 1). Further details pertaining to the data collection protocol, unit-cell parameters and structural refinement at 0.0001 GPa are reported in Tables 1-2-3.

H*P* data collections at different pressures (see Table 1) were performed, adopting the same experimental set-up, strategy and data treatment as those used at 0.0001 GPa. No violation of the reflection conditions of the *C*2/*m* symmetry was observed within the *P*-range investigated. Further details pertaining to the data collection protocol and H*P* structural refinements are given in Tables 1-2-3.

In-situ high-temperature powder diffraction data were collected at the CRG-BM08 "GILDA" beamline at ESRF using a translational image-plate and a hot air gas-blower (Meneghini et al. 2001). The powder sample was contained in a quartz-glass capillary. During the experiment, temperature on the hot air blower was directly measured by a thermocouple. Temperature has previously been calibrated by the *T*-induced phase transitions of quartz and $AgSO_4$, the melting point of NaCl and the thermal expansion of Al_2O_3, yielding a resulting *T*-uncertainty of ±2 °C. Diffraction data were integrated using the *Scan_Zero* software (written by Carlo Meneghini, ESRF). The unit-cell parameters obtained by Le Bail full-profile fit (Le Bail et al. 1988) using the GSAS software (Larson and Von Dreele 1994) at high temperature are given in Table 4. The whole diffraction pattern was fitted using the pseudo-Voigt profile function of Thomson et al. (1987), and the background curve was modeled using a 8-coefficients Chebyshev polynomial. Any attempt to perform a high-quality Rietveld structure refinement (Rietveld 1969) with the data collected at high temperature was unsuccessful.

Results: Elastic behaviour and structure evolution of clintonite at high-pressure

The evolution of the lattice parameters of the clintonite with pressure, based on the single-crystal diffraction data collected at PETRA III, is shown in Fig. 2. No phase transition has been observed within the pressure range investigated. Unit-cell volume data were fitted with a third-order Birch-Murnaghan EoS (Birch 1947; Angel 2000) using the EOS-FIT5.2 program (Angel 2001). The elastic parameters, simultaneously refined using the data weighted by the uncertainties in *P* and *V,* are: V_0= 457.1(2)Å^3, K_{T0}= 76(3)GPa and *K'*= 10.6(15). The evolution of the "Eulerian finite strain" *vs* "normalized stress" (*fe-Fe* plot; Angel 2000) is given in Fig. 2. The weighted linear regression through the data points yields *Fe*(0) = 76(3) GPa as intercept value and the slope of the regression line leads to a *K'* value of 10.6(8).

Axial bulk moduli were calculated with a "linearized" BM-EoS (Angel 2000). The refined elastic parameters are: a_0=5.210(1)Å, $K_{T0}(a)$=145(5)GPa and *K'*(*a*)= 4 (fixed) for the *a*-axis; b_0=

9.004(1) Å, $K_{T0}(b)$ = 184(9) GPa and $K'(b)$= 4 (fixed) for the *b*-axis; c_0= 9.899(1)Å, $K_{T0}(c)$ = 46(2) with $K'(c)$ = 4 (fixed) and $K_{T0}(c)$= 38(7) GPa with $K'(c)$=8(3) for the *c*-axis [$\beta(a) = 1/3K_{T0}(a)$ = 0.0023(1) GPa^{-1}; $\beta(b) = 1/3K_{T0}(b)$ = 0.0018(1) GPa^{-1}; $\beta(c) = 1/K_{T0}(c)$ = 0.0072(3) GPa^{-1}; $\beta(a) : \beta(b) : \beta(c)$ = 1.28 : 1 : 4.00]. The β-angle appears to increase in response to the applied *P* (Fig. 2), with: $\beta_P = \beta_0 + 0.033(4)P$.

The magnitude and orientation of the principal unit-strain coefficients, between room pressure and the maximum *P* achieved (ΔP= 10.1 GPa), were calculated with the STRAIN software (Ohashi 1982). The strain ellipsoid is oriented with the minor axis (ε_1) parallel to the *b*-axis and the major axis (ε_3) lying in the (010)-plane at 90.4(2)° from *a*, as shown in Fig. 1. The elastic behaviour of clintonite described on the basis of the unit-strain coefficients between 0.0001 and 10.1 GPa appears to be significantly anisotropic, being ε_1= -0.0014(2), ε_2= -0.0017(4), and ε_3 = -0.0053(2) GPa^{-1} ($\varepsilon_1 : \varepsilon_2 : \varepsilon_3$ = 1 : 1.21 : 3.78).

The structure refinements of clintonite up to 10.1 GPa show that, under hydrostatic pressure, the structure rearranges mainly compressing isotropically the inter-layer Ca-polyhedron, as shown by the evolution of the two independent Ca-O bond distances with *P* (*i.e.* Ca-O1 and Ca-O2, Table 3). The bulk-modulus of the Ca-polyhedron, described using a II-BM-EoS, is K_{T0}(Ca-polyhedron) = 41(2) GPa (Fig. 3). The compression of the bond distances between calcium and the basal oxygens of the tetrahedral sheet leads, in turn, to an increase of the ditrigonal distortion of the 6-membered ring of tetrahedral (6mR) with $\partial\alpha/\partial P \approx$ 0.1 °/GPa within the *P*-range investigated (Table 3, Fig. 3). The Mg-rich octahedra appear to compress in response of the applied pressure, though the scattering of the data within the *P*-range investigated does not allow an accurate calculation of the polyhedra bulk moduli (Fig. 3). Moreover, both the M1 and M2 octahedra tend to have a similar compressibility, approximately 115(10) GPa on the basis of a II-BM-EoS fit. In contrast, the tetrahedron appears to behave as a rigid unit up to 10 GPa (Table 3).

Results: Elastic behaviour of clintonite at high-temperature

The evolution of the lattice parameters of clintonite with temperature is shown in Fig. 4. No phase transition or anomalous thermo-elastic behaviour occurred within the *T*-range investigated, as shown by the monotonic evolution of the unit-cell volume and lattice parameters. The β angle appears to be almost constant (Fig. 4).

The axial and volume thermal-expansion coefficients were calculated following the protocol of Pawley et al. (1996) and Holland and Powell (1998). The evolution of the volume thermal expansion coefficient [*i.e.* $\alpha(T)=(1/V)(\partial V/\partial T)$] with *T* can be described by the polynomial function:

$$\alpha(T)= \alpha_0 + \alpha_1 T^{-1/2},$$

leading to:

$$V(T) = V_0\exp[\alpha_0(T\text{-}T_0) + 2\alpha_1(T^{1/2} - T_0^{1/2})] \approx V_0[1 + \alpha_0(T\text{-}T_0) + 2\alpha_1(T^{1/2} - T_0^{1/2})].$$

Fitting the experimental *V*-*T* data of clintonite reported in Table 4, we obtained:

$V(T)$ = 450.79(4) [1 + 2.78(4)·10^{-5}·T – 4.4(6)·10^{-5}·$T^{1/2}$], (*i.e.* α_0= 2.78(4)·10^{-5} °C^{-1} and α_1= – 4.4(6)·10^{-5} °C$^{1/2}$, $V(T)$ in Å^3 and T in °C).

Applying the same formalism to describe the axial thermo-elastic behavior, we obtained:

$a(T)$= 5.1940(3)·[1 + 1.01(2)·10^{-5}·T – 1.8(3)·10^{-5}·$T^{1/2}$] (*i.e.*$\alpha_0(a)$ = 1.01(2)·10^{-5}°C^{-1} and $\alpha_1(a)$= – 1.8(3)·10^{-5} °C$^{1/2}$);

$b(T)$=9.0002(4)·[1 + 1.07(1)·10^{-5}·T – 2.3(2)·10^{-5}·$T^{1/2}$] (*i.e.*$\alpha_0(b)$= 1.07(1)·10^{-5}°C^{-1} and $\alpha_1(b)$= – 2.3(2)·10^{-5}°C$^{1/2}$);

$c(T)$=9.7965(5)·[1 + 0.64(2)·10^{-5}·T – 7.3(30)·10^{-6}·$T^{1/2}$] (*i.e.*$\alpha_0(c)$= 0.64(2)·10^{-5}°C^{-1} and $\alpha_1(c)$= – 7.3(30)·10^{-6}°C$^{1/2}$).

An alternative and widely used description of the thermo-elastic behavior is based on a *V*-*T* fit with a quadratic function: $V(T)/V_0$= 1 + s_1·T + s_2·T^2, where s_1 and s_2 are refinable parameters. Fitting our experimental data, we obtained:

$V(T)/V_0$= 1 + 2.45(3)·10^{-5}·T + 1.1(3)·10^{-9}·T^2;

$a(T)/a_0$= 1 + 8.7(1)·10^{-6}·T + 5(1)·10^{-10}·T^2;

$b(T)/b_0$= 1 + 8.8(1)·10^{-6}·T + 7(1)·10^{-10}·T^2;

$c(T)/c_0$= 1 + 7.3(1)·10^{-6}·T - 6(1)·10^{-10}·T^2,

with an anisotropic scheme: $s_1(a)$: $s_1(b)$: $s_1(c)$ = 1.19 : 1.21 : 1.

The magnitude and orientation of the principal unit-strain coefficients, between 25 and 960 °C (ΔT= 935 K), were calculated using STRAIN (Ohashi 1982). The unit-strain ellipsoid is oriented with ε_1 parallel to the *b*-axis, and ε_2 and ε_3 lying in the (010)-plane, with ε_3^*a*=95(3)° (Fig. 1). The thermo-elastic behaviour of clintonite described on the basis of the unit-strain coefficients between 25 and 960°C is not significantly anisotropic, with ε_1= 0.95(2)·10^{-5} °C^{-1}, ε_2=0.91(3)·10^{-5} °C^{-1}, and ε_3=0.66(1)·10^{-5} °C^{-1}, with ε_1: ε_2: ε_3 = 1.44 : 1.38 : 1.

Discussion and conclusions

This is the first experiment aimed to describe the thermo-elastic behavior and the *P*-induced structure evolution of a *brittle* mica.

The single-crystal structure refinement based on the diffraction data collected at 0.0001 GPa provides a structure model comparable to those previously reported (*e.g.* Joswig et al. 1986; MacKinney et al. 1988; Alietti et al. 1997). The inter-layer site is fully occupied by Ca, according to

the EMPA-WDS analysis. The Ca-octahedron is almost regular, as shown by the two independent Ca-O bond distances (Table 3). The refined occupancy factor of the M1 and M2 octahedral sites, modeled with the scattering factor of Mg alone, shows the presence of Al (or Fe) along with Mg (*i.e. s.o.f.* (M1) = 12.48 e^- and *s.o.f.* (M2) = 12.41 e^-). The M1 and M2 octahedral bond distances suggest that Fe likely share the M1 site along with Mg and Al (Table 3), according to experimental findings of Joswig et al. (1986). The tetrahedral bond distances confirm that Si and Al are randomly distributed, and the chemical analysis shows an Al/Si content (a.p.f.u.) higher than 2.3. This experiment delivers a further evidence of the violation of the Loewenstein's aluminum avoidance rule (Loewenstein 1954) in a natural material, due to the Al/Si (a.p.f.u.) > 2. Such a violation, along with those previously reported for several synthetic materials, suggests that the "Loewenstein's rule" is not universally valid, and so it is should not be considered as a "rule". The ditrigonal rotation angle in clintonite at 0.0001 GPa is significantly high ($\alpha(P_0)$ = 23.00(4)°, Table 3), as previously observed (*e.g.* Joswig et al. 1986; MacKinney et al. 1988; Alietti et al. 1997).

The H*P* single-crystal data allowed the description of the elastic behavior of clintonite to about 10 GPa. Magnitude and orientation of the unit-strain ellipsoid show that the lowest compression is observed along [010] (*i.e.* stiffest direction, $\varepsilon_1 \| b$), whereas the highest compression occurs on the (010)-plane, with the softest direction, ε_3, oriented with $\varepsilon_3 \hat{} a$ = 90.4(2)° and $\varepsilon_3 \hat{} c$ = 9.7(2)° (Fig. 1). The elastic anisotropy in response to hydrostatic pressure (with: ε_1: ε_2: ε_3 ~ 1 : 1.1 : 3.8) is pronounced, as observed in other phyllosilicates (*e.g.* Zanazzi and Pavese 2002 for a review; Pavese et al. 2003, 2007; Comodi et al. 2004; Curetti et al. 2006; Gatta et al. 2011). However, it appears that in clintonite the softest direction is not parallel to [001], as $\varepsilon_3 \hat{} c$ = 9.7(2)°. If we compare the elastic behavior of clintonite with that of *true micas*, we observe that clintonite is significantly stiffer than phlogopites [*e.g.* phlogopite-1*M* : K_{T0}= 49.7(5)GPa and *K'*=8.59(19), Pavese et al. 2003; K_{T0}= 54(2)GPa and *K'*=7(1), Comodi et al. 2004; phlogopite-3*T* : K_{T0}= 42.8(29)GPa and *K'*= 9.9(17), Gatta et al. 2011] and phengites [*e.g.* 3*T*-polytype: K_{T0}=60.4(7) GPa and K_0'=5.79(11), Curetti et al. 2006]. A common feature among phyllosilicates is the high *K'* value, as observed also in clintonite (*i.e. K'*= 10.6(15)).

The H*T* powder data collected up 960°C showed a not so pronounced anisotropic thermo-elastic behavior of clintonite, as usually expected in phyllosilicates (*e.g.* Zanazzi and Pavese 2002 for a review), with ε_1: ε_2: ε_3 = 1.44 : 1.38 : 1. In this case, ε_1 is parallel to [010] (*i.e.* the most expandable direction), whereas ε_2 and ε_3 lie in the (010)-plane, with $\varepsilon_3 \hat{} a$=95(3)° and $\varepsilon_3 \hat{} c$=5(3)° (Fig. 1). The orientation of the thermal unit-strain ellipsoid differs significantly from those that can be deduced on the basis of the H*T*-data previously reported for *true micas* (*e.g.* Catti et al. 1989; Guggenheim et al. 1987; Mookherjee et al. 2001; Pavese et al. 1997, 1999, 2003; Russell and

Guggenheim 1999; Comodi and Zanazzi 2000; Chon et al. 2003; Gemmi et al. 2008, Ventruti et al. 2008), in which the most expandable direction is parallel to [001]. Furthermore, clintonite shows an uncommon stability at high temperature, as no structure collapsing in response to the *T*-induced dehydroxylation occurs at least up to 960 °C. In *true micas*, the dehydroxylation process usually occurs at lower temperature (*e.g.* ~520-720 °C in phengites, Gemmi et al. 2008; ~600 °C in paragonite, Comodi and Zanazzi 2000; ~600°C in phlogopite, Ventruti et al. 2008). The volume thermal-expansion coefficient of clintonite up to 960°C is: $\alpha(T)= \alpha_0 + \alpha_1 T^{-1/2} = 2.78(4)\cdot10^{-5} - 4.4(6)\cdot10^{-5} T^{-1/2}$ (*sensu* Pawley et al. 1996, Holland and Powell 1998).

If we combine the thermo-elastic parameters obtained in this study, a *P*-*T*-*V* EoS of clintonite can be obtained:

$V_{(P,T)} \sim V_{(P0,T0)}[1 - \beta\Delta P + \alpha\Delta T] = V_{(P0,T0)}[1 - 0.0131(4)\cdot\Delta P + 2.78(4)\cdot10^{-5}\cdot\Delta T]$

(with $\beta = 1/K_{T0}$ in GPa^{-1} and α in $°C^{-1}$).

The H*P*- and H*T*-data of this study show that in clintonite the most and the less expandable directions do not correspond to the most and the less compressible directions, respectively. The pronounced compressibility in K (or Na, Cs, Rb) micas along [001] (Zanazzi and Pavese 2002, Comodi et al. 2003) is mainly governed by the compression of the inter-layer cation to basal oxygens of the tetrahedral sheet bond-distances, due to the comparatively weak cation-oxygen bonds of the inter-layer with respect to the intra-octahedral or intra-tetrahedral ones. However, in K micas, an anisotropic compression mechanism of the inter-layer polyhedron occurs, with the shortest K-O bond-distances being more compressible than the longest ones (*e.g.* Comodi et al. 2004, Gatta et al. 2009, 2010). As a consequence, the ditrigonal distortion of the 6mR is significantly more pronounced in *true* micas than in *brittle* micas in response to applied pressure (*e.g.* $\partial\alpha/\partial P \approx 0.6$-$0.7$ °/GPa, with $\alpha(P_0) \approx 5$-$6°$ in phengites, Gatta et al. 2009, 2010). As highlighted by Gatta et al. (2010), the ditrigonal distortion is probably the most *P*-induced energy-convenient mechanism to make octahedral- and tetrahedral-sheets match one another so as to form the T-M-T layer. An increase of the ditrigonal rotation tends to favour the trigonal anti-prismatic (ideal octahedral) coordination in the octahedral sheet, acting as a possible stabilization factor of the structure (Ferraris and Ivaldi 2002). In clintonite, $\alpha(P_0)$ is significantly higher than that observed in K micas at room-*P* (*i.e.* 23° in clintonite, <11° in phengites and phlogopites), and the ditrigonalization process is less pronounced in response to the applied pressure. Considering *a*) the high value of α in clintonite at room-*P* and *b*) that the maximum value expected for α is 30° (Ferraris and Ivaldi 2002), it is not surprising that clintonite experiences a ditrigonalization process which is significantly modest (with $\partial\alpha/\partial P \approx 0.1$ °/GPa; Fig. 3, Table 3) if compared to that observed in *true micas*.

The less pronounced ditrigonalization of the 6mR in clintonite is the effect of the bivalent nature of the inter-layer cation and its almost ideal coordination shell (almost perfect octahedron, Table 3). The compressibility of the Ca-octahedron is, in addition, significantly different than that of the K-polyhedron in *true micas* (*i.e.* K_{T0}(Ca-polyhedron) = 41(2) GPa, this study; K_{T0}(K-polyhedron) = 26(1) GPa, Gatta et al. 2010).

In *true micas*, an increase of temperature is usually followed by a decrease of α, leading to a regularization of the 6mR configuration (Ferraris and Ivaldi 2002; Zanazzi and Pavese 2002; Gemmi et al. 2008). In this study, we do not have structure data at high temperature, and this hinders a description of the mechanisms that govern, at the atomic scale, the H*T* elastic anisotropy, which is of about 40% (*i.e.* ε_1: ε_2: ε_3 = 1.44 : 1.38 : 1, with ε_1||[010] and ε_3^*a*=95(3)°). However, some implications can be drawn on the basis of the crystal structure of clintonite at room-*T*. The equatorial plane of the inter-layer Ca-octahedron (through the four O2 atoms) forms an angle of ~ 20° with [001] (Fig. 1). This orientation can lead to a more pronounced thermal expansion of the structure on (001), rather than along [001], only if an anisotropic expansion of the Ca-polyhedron occurs mainly along the longest axis (*i.e.* O1↔O1 ~ 4.911 at room-*T*) (Fig. 1). Such an hypothetical anisotropic expansion of the Ca-polyhedron does not reflect the compressional behaviour of the polyhedron, which, in turn, appears to be almost isotropic (Table 3).

Acknowledgements

This work was funded by the Italian Ministry of University and Research, MIUR-Project: 2008SPZ743. The authors warmly thank Paolo Lotti for his assistance during the H*P* data treatment, PETRA-III (Hamburg) and ESRF (Grenoble) for the allocation of synchrotron beam time. Two reviewers and the Editor M. Rieder are thanked for their suggestions.

References

Alietti E, Brigatti MF, Poppi L (1997) Clintonite-1*M*: Crystal chemistry and its relationships to closely associated Al-rich phlogopite. Am Mineral 82:936-945.

Angel RJ (2000) Equation of State. In R.M. Hazen, R.T. Downs, Eds., High-Temperature and High-Pressure Crystal Chemistry, Reviews in Mineralogy and Geochemistry, Vol. 41, pp 35-59. Mineralogical Society of America and Geochemical Society, Washington, DC, U.S.A..

Angel RJ (2001) EOS-FIT V6.0.Computer program**.** Crystallography Laboratory, Dept. Geological Sciences, Virginia Tech, Blacksburg, U.S.A..

Angel RJ, Bujak M, Zhao J, Gatta GD, JacobsenSD (2007) Effective hydrostatic limits of pressure media for high-pressure crystallographic studies. J Appl Crystallogr 40:26–32.

Annersten H, Olesch M (1978) Distribution of ferrous and ferric iron in clintonite and the Mössbauer characteristic of ferric iron in tetrahedral coordination. Can Mineral 16:199-203.

Bailey SW (1988) X-ray diffraction identification of the polytypes of mica, serpentine and chlorite Clays Clay Minerals 36:195-213.

Balic-Zunic T, Vickovic I (1996) IVTON (Version 2) - Program for the calculation of geometrical aspects of crystal structures and some crystal chemical applications. J Appl Crystallogr 29:305-306.

Birch F (1947) Finite elastic strain of cubic crystal. Phys Rev 71:809-824.

Brigatti MF, Guggenheim S (2002) Mica crystal chemistry and the influence of pressure, temperature, and solid solution on atomistic models. In A. Mottana, F.P. Sassi, J.B. Thompson, Jr., S. Guggenheim, Eds., Micas: Crystal Chemistry and Metamorphic Petrology, Review in Mineralogy and Geochemistry, Vol. 46, p. 1-97. Mineralogical Society of America and Geochemical Society, Washington, DC, U.S.A..

Catti M, Ferraris G, Ivaldi G (1989) Thermal strain analysis in the crystal structure of muscovite at 700°C. Eur J Mineral 1:625–632.

Chon C-H, Kim SA, Moon H-S (2003) Crystal structure of biotite at high temperatures and of heat-treated biotite using neutron powder diffraction. Clays Clay Miner 51:519–528.

Comodi P, Zanazzi PF (2000) Structural thermal behaviour of paragonite and its dehydroxylate: a high temperature single crystal study. Phys Chem Miner 27:377–385.

Comodi P, Drábek M, Montagnoli M, Rieder M, Weiss Z, Zanazzi PF (2003) Pressure-induced phase transition in synthetic trioctahedral Rb-mica. Phys Chem Minerals 30:198-205.

Comodi P, Fumagalli P, Montagnoli M, Zanazzi PF (2004) A single-crystal study on the pressure behavior of phlogopite and petrological implications. Am Mineral 89:647-653.

Curetti N, Levy D, Pavese A, Ivaldi G (2006) Elastic properties and stability of coexisting 3*T* and $2M_1$ phengite polytypes. Phys Chem Minerals 32:670–678.

Farmer VC, Velde G (1973) Effects of structural order and disorder on the infrared spectra of brittle micas. Min Mag 39:282-288.

Ferraris G, Ivaldi G (2002) Structural features of micas. In A. Mottana, F.P. Sassi, J.B. Thompson, Jr., S. Guggenheim, Eds.,Micas: Crystal Chemistry and Metamorphic Petrology, Review in Mineralogy and Geochemistry, Vol. 46, p. 117-53. Mineralogical Society of America and Geochemical Society, Washington, DC, U.S.A..

Forman SA, Kodama H., Abbey S. (1967) A re-examination of xanthophyllite [clintonite] from the type locality. Can Mineral 9:25-30.

Gatta GD, Rotiroti N, Pavese A, Lotti P, Curetti N (2009) Structural evolution of a 3*T* phengite mica up to 10 GPa: an *in-situ* single-crystal X-ray diffraction study. Z Kristallogr 224:302-310.

Gatta GD, Rotiroti N, Pavese A, Lotti P, Curetti N (2010) Structural evolution of a 2M1 phengite mica up to 11 GPa: an in-situ single-crystal X-ray diffraction study. Phys Chem Minerals 37:581-591.

Gatta GD, Merlini M, Rotiroti N, Curetti N, Pavese A (2011) On the crystal chemistry and elastic behavior of a phlogopite 3*T*. Phys Chem Minerals 38:655-664.

Gemmi M, Merlini M, Pavese A, Curetti N (2008) Thermal expansion and dehydroxylation of phengite micas. Phys Chem Minerals 35:367–379.

Guggenheim S (1984) The brittle micas. In SW Bailey, Ed., Micas, Reviews in Mineralogy, Vol. 13, p. 61-104. Mineralogical Society of America, Washington, DC, U.S.A..

Guggenheim S, Bailey SW (1975) Refinement of margarite structure in subgroup symmetry. Am Mineral 60:1023-1029.

Guggenheim S, Bailey SW (1978) Refinement of margarite structure in subgroup symmetry: correction, further refinement, and comments. Am Mineral 63:186-1987.

Guggenheim S, Chang YH, Koster van Groos AF (1987) Muscovite dehydroxylation: high-temperature studies. Am Mineral 72:537–550.

Holland TJB, Powell R (1998) An internally consistent thermodynamic data set for phases of petrological interest. J Metamorphic Geol 16:309-343.

Houzar S, Novák M (2006) Clintonite-bearing assemblages in chondrodite marbles from the contact aureole of the Třebíč Pluton, Moldanubian Zone, Bohemian Massif. J Czech Geol Soc 51:249-258.

Raymond J (1976) High-temperature contact metamorphism of carbonate rocks in a shallow crystal environment, Christmas Mountains, Big Bend region, Texas. Am Mineral 61:776-781.

Joswig W, Takéuchi Y, Fuess H (1983) Neutron-diffraction study on the orientation ofhydroxyl groups in margarite. Z Kristallogr 165:295-303.

Joswig W, Amthauer G, Takéuchi Y (1986) Neutron diffraction and Mössbauer spectroscopic study of clintonite (xanthophyllite). Am Mineral 71:1194-1197.

Kushiro I, Yoder HS (1964) Breakdown of monticellite and akermanite at high pressure. Carnegie Inst. Wash. Year Book 63:81.83.

Larson AC, Von Dreele RB (1994) General Structure Analysis System(GSAS), Los Alamos National Laboratory Report LAUR 86-748.

Le Bail A, Duroy H, Fourquet JL (1988) Ab-initio structure determination of $LiSbWO_6$ by X-ray powder diffraction. Mat Res Bull 23:447-452.

Loewenstein W (1954) The distribution of aluminum in the tetrahedral of silicates and aluminates. Am Mineral 39:92-96.

MacKinney JA, Mora CI, Bailey SW (1988) Structure and crystal chemistry of clintonite. Am Mineral 73:365-375.

Mao HK, Xu J, Bell PM (1986) Calibration of the ruby pressure gauge to 800 kbar under quasi-hydrostatic conditions. J Geophys Res 91:4673-4676.

Meneghini C, Artioli G, Balerna A, Gualtieri AF, Norby P, Mobilio S (2001) Multipurpose imaging-plate camera for in-situ powder XRD at the GILDA beamline. J Synchrotron Rad 8:1162-1166.

Mookherjee M, Redfern SAT, Zhang M (2001) Thermal response of structure and hydroxyl ion of phengite-2M1. Eur J Mineral 13:545–555.

Nespolo M, Ferraris G (2001) Effects of the stacking faults on the calculated electron density of mica polytypes – The Ďurovič effect. Eur J Mineral 13:1035-1045.

Nespolo M, Ďurovič S (2002) Crystallographic basis of polytypism and twinning in micas. In A. Mottana, F.P. Sassi, J.B. Thompson, Jr., S. Guggenheim, Eds., Micas: Crystal Chemistry and Metamorphic Petrology, Review in Mineralogy and Geochemistry, Vol. 46, p. 155-279. Mineralogical Society of America and Geochemical Society, Washington, DC, U.S.A..

Ohashi Y (1982) STRAIN: A program to calculate the strain tensor from two sets of unit-cell parameters. In: Hazen RM, Finger LW, Comparative Crystal Chemistry, John Wiley & Sons, New York, 92-102.

Olesch M (1975) Synthesis and solid solubility of trioctahedral brittle micas in the system CaO-MgO-A_2O_3-SiO_2-H_2O Am Mineral 60:188-199.

Olesch M, Seifert F (1976) Stability and phase relations of trioctahedral calcium brittle micas (clintonite group). J Petrology 17:291-314.

Oxford Diffraction (2010) Oxford Diffraction Ltd., Xcalibur CCD system, CrysAlis Software system.

Pavese A, Ferraris G, Prencipe M, Ibberson R (1997) Cation site ordering in phengite 3*T* from the Dora-Maira massif (western Alps): a variable-temperature neutron powder diffraction study. Eur J Mineral 9:1183–1190.

Pavese A, Ferraris G, Pischedda V, Mezouar M (1999b) Synchrotron powder diffraction study of phengite 3*T* from the Dora-Maira massif: *P-V-T* equation of state and petrological consequences. Phys Chem Miner 26:460–467.

Pavese A, Levy D, Curetti N, Diella V, Fumagalli P, Sani A (2003) Equation of state and compressibility of phlogopite by in-situ high-pressure X-ray powder diffraction. Eur J Mineral 15:455-463.

Pavese A,Curetti N,Diella V,Levy D, Dapiaggi M, Russo U (2007) *P-V* and *T-V* Equations of State of natural biotite: An in-situ high-pressure and high-temperature powder diffraction study, combined with Mössbauer spectroscopy. Am Mineral 92:1158-1164.

PawleyAR, Redfern SAT, Holland TJB (1996) Volume behaviour of hydrous minerals at high pressure and temperature: 1. Thermal expansion of lawsonite, zoisite, clinozoisite, and diaspore. Am Mineral 81:335-340.

Rice JM (1979) Petrology of clintonite-bearing marbles in Boulder Aureole, Montana. Am Mineral 64:519-526.

Rietveld HM (1969) A profile refinement method for nuclear and magnetic structures. J Appl Crystallogr 2:65–71.

Russell RL, Guggenheim S (1999) Crystal structures of near-endmember phlogopite at high temperatures and heat-treated Fe-rich phlogopite: the influence of the O, OH, F site. Can Mineral 37:711–720.

Sanero E (1940) La struttura della xantophyllite. Period Mineral 11:53-77.

Sugaki A, Campos E, Kojima S (2000) Mineralogy of the Panulcillo skarn copper deposit, Coquimbo Region, Chile. Rev Geol Chile 27:139-155.

Sheldrick GM (1997) SHELX-97. Programs for crystal structure determination and refinement. University of Göttingen, Germany.

Takéuchi Y (1966) Structural studies of brittle micas (I). The structure of xanthophyllite refined. Mineralogical Joumal 4:424-437.

Takéuchi Y, Sadanaga R (1959) The crystal structure of xanthophyllite. Acta Crystallogr 12:945-946.

Thomson P, CoxDE, Hastings JB (1987) Rietveld refinement of Debye-Scherrer synchrotron X-ray data from Al_2O_3.J Appl Crystallogr 20:79-83.

Tracy RJ (1979) Monticellite marble at Cascade Mountain, Adirondack Mountains, New York. Am Mineral 63:991-999.

Ulmer P (1982) Monticellite-clintonite bearing assemblages at the southern border of the Adamello-Massif. Rend Soc Ital Mineral Petrogr 38:617-628.

Ventruti G, Zema M, Scordari F., Pedrazzi G (2008) Thermal behavior of a Ti-rich phlogopite from Mt.Vulture (Potenza, Italy): An in situ X-ray single-crystal diffraction study. Am Mineral 93:632–643.

Warner RD, Luth WC (1973) Two phase data for the join monticellite ($CaMgSiO_4$) - forsterite (Mg_2SiO_4): experimental results and numerical analysis. Am Mineral 58:998-1008.

Wilson AJC, Prince E. (1999) International Tables for X-ray Crystallography, Volume C: Mathematical, physical and chemical tables (2nd Edition), Kluwer Academic, Dordrecht, NL.

Woodford DT, Sisson VB, Leeman WP (2001) Boron metasomatism of the Alta stock contact aureole, Utah: Evidence from borates, mineral chemistry, and geochemistry. Am Mineral 86:513–533.

Zanazzi PF, Pavese A (2002) Behavior of micas at high pressure and high temperature. In A. Mottana, F.P. Sassi, J.B. Thompson, Jr., S. Guggenheim, Eds., Micas: Crystal Chemistry and Metamorphic Petrology, Review in Mineralogy and Geochemistry, Vol. 46, p. 99-116. Mineralogical Society of America and Geochemical Society, Washington, DC, U.S.A..

Figure 1. Crystal structure of clintonite, based on the single-crystal structure refinement at room *P/T* of this study, and orientation of the unit-strain ellipsoids with ΔP = 10.1 GPa (green) and ΔT = 935°C (orange).

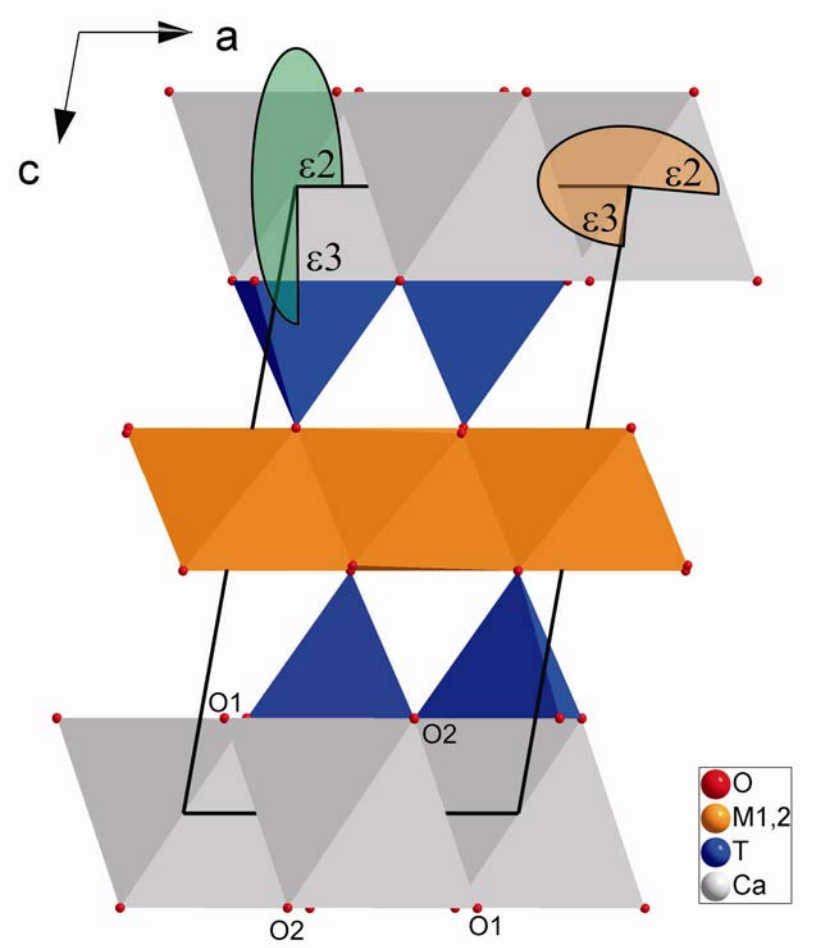

Figure 2. Evolution of the lattice parameters of clintonite with pressure; the solid lines represent the BM-EoS fit for the *a*, *b* and *c*-axis and for the unit-cell volume (see text for details) and the weighted polynomial regression through the data points for the β angle. Evolution of the "normalized stress" ($Fe = P/[3fe(1+2fe)^{5/2}]$) *vs.* Eulerian finite strain ($fe = [(V_0/V)^{2/3} - 1]/2$); the solid line is a weighted linear fit through the data.

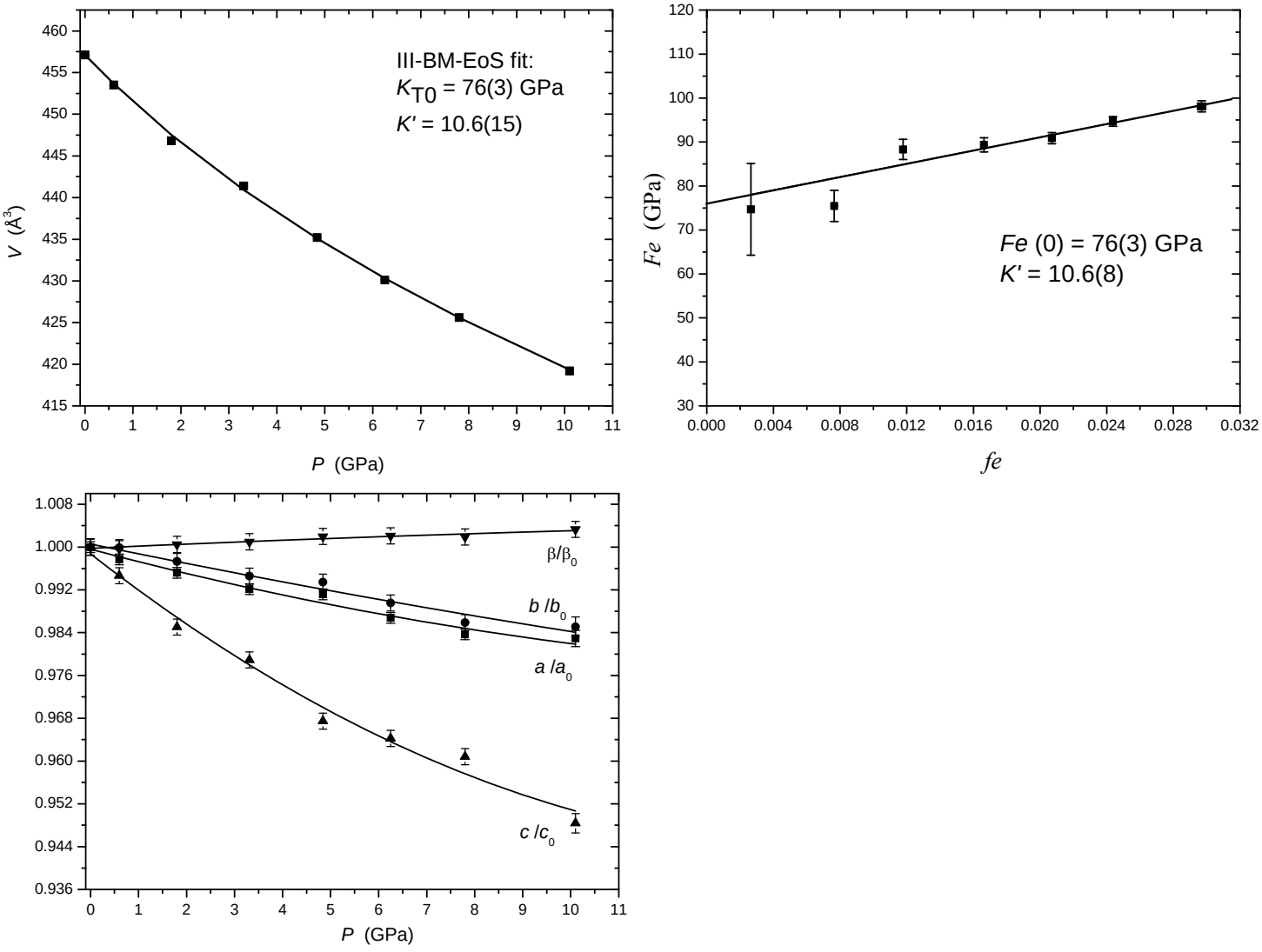

Figure 3. Evolution of the polyhedral volume with pressure of the Ca, M1 and M2 polyhedra; for the Ca-polyhedron, the solid line represents the BM-EoS fit. Evolution of the ditrigonal distortion angle α with *P* up to 7.8 GPa (the data point at 10.1 GPa is out of trend).

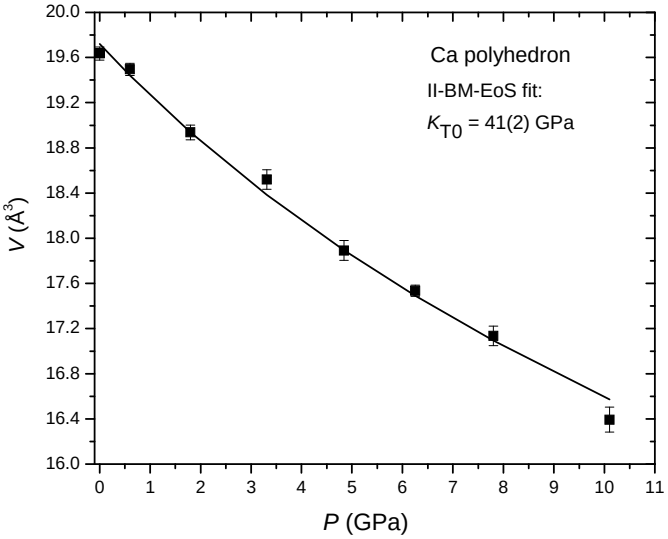

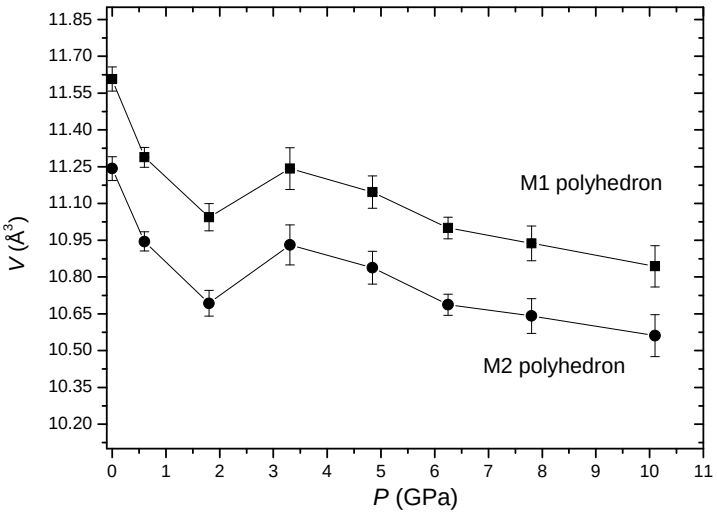

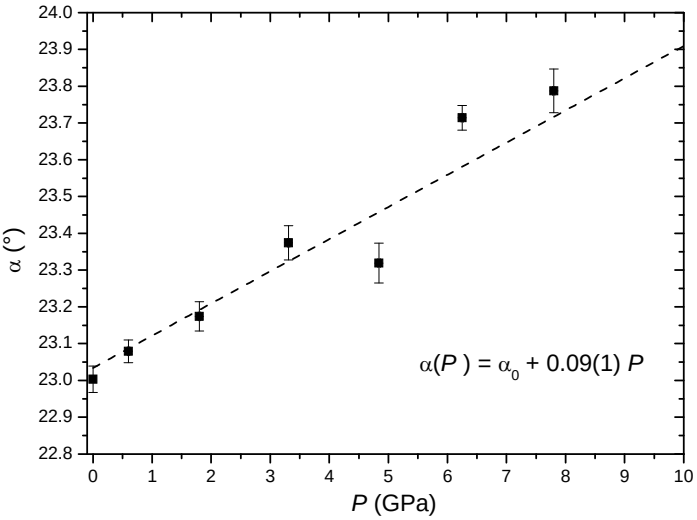

Figure 4. Evolution of the unit-cell parameters of clintonite with temperature. For *a*, *b*, *c* and *V*, the solid lines represent the fit of the equation $V(T) \approx V_0[1 + \alpha_0(T\text{-}T_0) + 2\alpha_1(T^{1/2}\text{–}T_0^{1/2})]$ to the *V*-*T* data and $l(T) \approx l_0[1 + \alpha_0(T\text{-}T_0) + 2\alpha_1(T^{1/2}\text{–}T_0^{1/2})]$ to the (*a*,*b*,*c*)-*T* data, respectively.

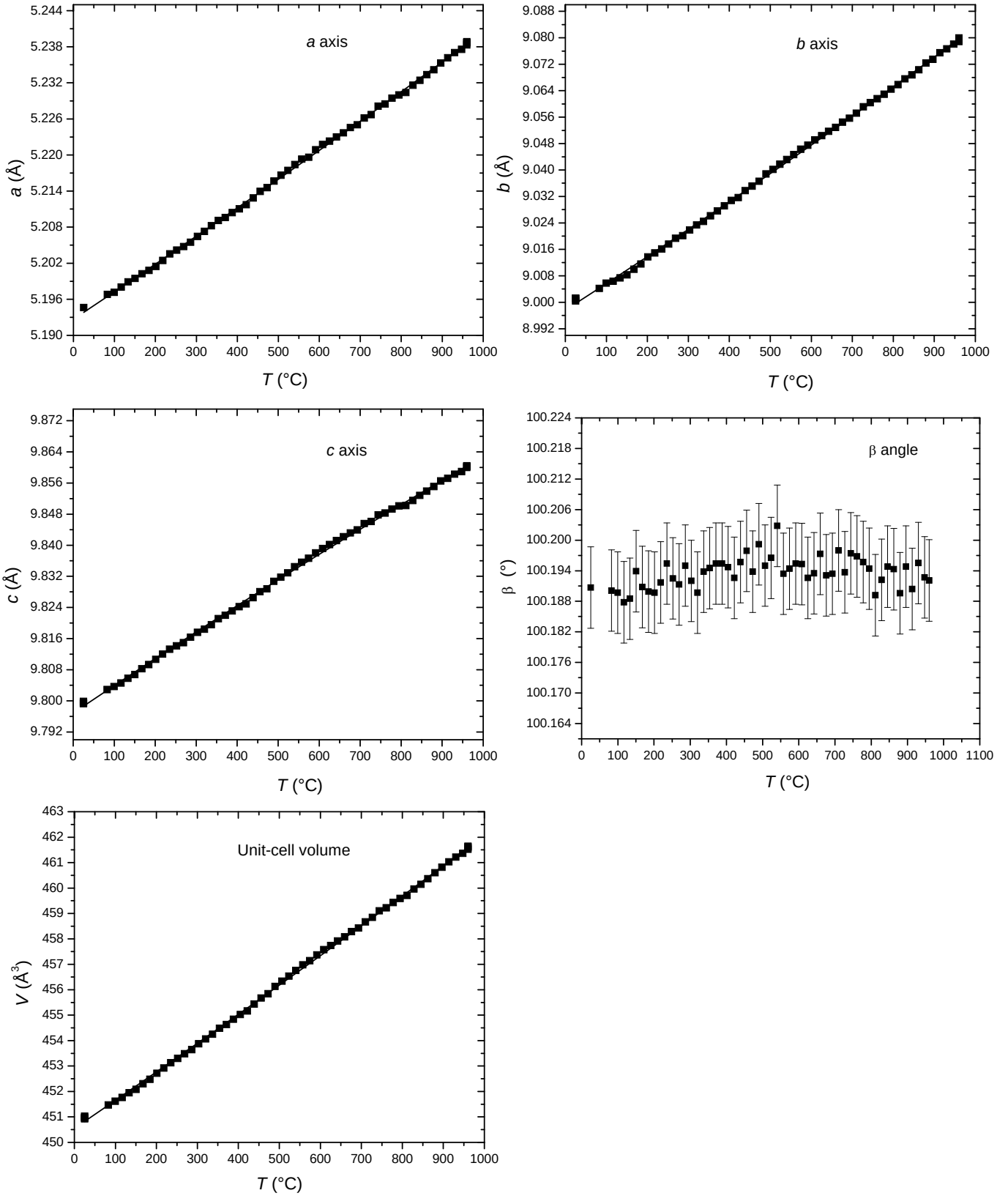

Table 1. Data pertaining to the data collections and structure refinements of clintonite at different pressures

P (GPa)	0.0001*	0.60(8)	1.80(8)	3.31(8)	4.84(8)	6.25(8)	7.80(8)	10.1(8)
X-ray radiation	0.29036(1)	0.29036(1)	0.29036(1)	0.29036(1)	0.29036(1)	0.29036(1)	0.29036(1)	0.29036(1)
Z	2	2	2	2	2	2	2	2
Scan type	ω	ω	ω	ω	ω	ω	ω	ω
Scan width (°/frame)	1	1	1	1	1	1	1	1
Exposure (s/frame)	1	1	1	1	1	1	1	1
Space Group	*C* 2/*m*	*C* 2/*m*	*C* 2/*m*	*C* 2/*m*	*C* 2/*m*	*C* 2/*m*	*C* 2/*m*	*C* 2/*m*
a (Å)	5.210(1)	5.198(1)	5.185(1)	5.169(1)	5.164(1)	5.141(1)	5.125(1)	5.121(2)
b (Å)	9.004(1)	9.003(1)	8.980(1)	8.955(1)	8.945(1)	8.910(1)	8.877(1)	8.870(2)
c (Å)	9.899(1)	9.846(1)	9.751(1)	9.690(1)	9.577(1)	9.545(1)	9.511(1)	9.388(2)
β (°)	100.16(1)	100.13(1)	100.21(1)	100.26(1)	100.36(1)	100.37(1)	100.35(1)	100.49(1)
V (Å^3)	457.1(1)	453.5(1)	446.8(1)	441.4(1)	435.2(1)	430.1(1)	425.6(1)	419.2(3)
Maximum 2θ (°)	23.90	23.95	24.02	24.10	23.88	23.87	23.95	23.81
Measured reflections	622	599	566	532	506	578	576	525
Unique reflections	242	281	279	200	230	249	223	213
Unique reflections with $F_0 > 4\sigma(F_0)$	227	263	256	192	215	235	209	199
R_{int}	0.0112	0.0099	0.0236	0.0104	0.0221	0.0100	0.0112	0.0211
N. of refined parameters	25	25	25	25	25	25	25	25
R_1, $F_0>4\sigma(F_0)$	0.0300	0.0264	0.0384	0.0356	0.0418	0.0265	0.0437	0.0564
R_1, all reflections	0.0320	0.0286	0.0410	0.0364	0.0451	0.0284	0.0457	0.0583
wR^2	0.0869	0.0783	0.0990	0.1081	0.1157	0.0799	0.1309	0.1481
Residuals (e^-/ Å^3)	-0.35/+0.36	-0.29/+0.27	-0.35/+0.53	-0.51/+0.47	-0.48/+0.37	-0.30/+0.35	-0.63/+0.63	-0.67/+0.60

$R_{int}=\Sigma|F_{obs}^2-F_{obs}^2{}_{(mean)}|/\Sigma[F_{obs}^2]$; $R_1=\Sigma(|F_{obs}|-|F_{calc}|)/\Sigma|F_{obs}|$; $wR_2=[\Sigma[w(F^2_{obs}-F^2_{calc})^2]/\Sigma[w(F^2_{obs})^2]]^{0.5}$, $w=1/[\sigma^2(F_{obs}^2)+(0.04*P)^2]$, $P=(\mathrm{Max}(F_{obs}^2,0)+2*F_{calc}^2)/3$.

Table 2. Atomic coordinates and isotropic thermal displacement parameters ($Å^2$) at different pressures. The refined site occupancy factors of the M1 and M2 sites is given (in e^-).

	x/a	*y/b*	*z/c*	U_{iso}
P=0.0001 GPa				
T(Al)	0.0700(2)	0.16695(6)	0.2091(2)	0.0032(3)
Ca	0	0.5	0	0.0096(3)
M1(Mg, 12.48e^-)	0	0	0.5	0.0045(6)
M2(Mg, 12.41e^-)	0	0.3294(1)	0.5	0.0032(5)
O1	-0.0722(6)	0	0.1511(9)	0.0123(6)
O2	0.3614(4)	0.1887(2)	0.1506(6)	0.0117(5)
O3	0.1302(4)	0.1684(2)	0.3852(7)	0.0101(5)
OH	0.1277(6)	0.5	0.3940(9)	0.0109(6)
P=0.60(8) GPa				
T(Al)	0.07006(12)	0.16696(6)	0.2094(2)	0.0043(3)
Ca	0	0.5	0	0.0110(3)
M1(Mg, 12.19 e^-)	0	0	0.5	0.0048(5)
M2(Mg, 12.34 e^-)	0	0.32952(8)	0.5	0.0042(4)
O1	-0.0726(5)	0	0.1519(8)	0.0138(5)
O2	0.3618(4)	0.1886(2)	0.1509(6)	0.0133(4)
O3	0.1307(3)	0.1682(1)	0.3875(6)	0.0121(4)
OH	0.1278(5)	0.5	0.3958(8)	0.0131(5)
P=1.80(8) GPa				
T(Al)	0.06992(18)	0.16682(8)	0.2086(3)	0.0095(3)
Ca	0	0.5	0	0.0159(4)
M1(Mg, 12.19 e^-)	0	0	0.5	0.0096(7)
M2(Mg, 12.43 e^-)	0	0.3297(1)	0.5	0.0098(5)
O1	-0.0733(7)	0	0.1513(10)	0.0185(8)
O2	0.3619(5)	0.1882(2)	0.1493(7)	0.0187(6)
O3	0.1315(5)	0.1682(2)	0.3870(8)	0.0169(6)
OH	0.1287(7)	0.5	0.3973(10)	0.0198(8)
P=3.31(8) GPa				
T(Al)	0.0694(3)	0.1669(1)	0.2072(5)	0.0025(5)
Ca	0	0.5	0	0.0083(5)
M1(Mg, 12.34 e^-)	0	0	0.5	0.0035(8)
M2(Mg, 12.38 e^-)	0	0.32973(13)	0.5	0.0022(6)
O1	-0.0744(8)	0	0.1496(14)	0.0115(8)
O2	0.3621(7)	0.1875(2)	0.1487(10)	0.0114(7)
O3	0.1302(7)	0.1681(2)	0.3846(14)	0.0096(7)
OH	0.1279(8)	0.5	0.3934(14)	0.0114(8)
P=4.84(8) GPa				
T(Al)	0.0682(2)	0.1668(1)	0.2044(4)	0.0062(5)
Ca	0	0.5	0	0.0115(5)
M1(Mg, 12.43 e^-)	0	0	0.5	0.0069(8)
M2(Mg, 12.46 e^-)	0	0.33006(14)	0.5	0.0063(6)
O1	-0.0755(9)	0	0.1467(14)	0.0155(9)
O2	0.3602(7)	0.1876(3)	0.1453(10)	0.0153(7)
O3	0.1301(7)	0.1677(2)	0.3844(11)	0.0129(7)
OH	0.1262(9)	0.5	0.3918(13)	0.0150(9)
P=6.25(8) GPa				
T(Al)	0.06892(14)	0.16687(6)	0.2057(2)	0.0036(3)
Ca	0	0.5	0	0.0090(3)
M1(Mg, 12.38 e^-)	0	0	0.5	0.0044(5)
M2(Mg, 12.43 e^-)	0	0.33006(9)	0.5	0.0036(4)
O1	-0.0784(5)	0	0.1471(8)	0.0131(6)
O2	0.3620(4)	0.1868(2)	0.1460(6)	0.0125(4)
O3	0.1297(4)	0.1680(2)	0.3844(7)	0.0102(5)
OH	0.1267(5)	0.5	0.3925(8)	0.0121(6)
P=7.80(8) GPa				
T(Al)	0.0688(3)	0.1668(1)	0.2053(4)	0.0027(5)
Ca	0	0.5	0	0.0079(6)
M1(Mg, 12.14 e^-)	0	0	0.5	0.002(1)
M2(Mg, 12.43 e^-)	0	0.3302(1)	0.5	0.0022(8)
O1	-0.0790(10)	0	0.1460(15)	0.013(1)
O2	0.3611(7)	0.1863(3)	0.1443(11)	0.0110(8)
O3	0.1296(7)	0.1679(3)	0.3839(11)	0.0099(9)
OH	0.1267(9)	0.5	0.3916(14)	0.011(1)
P=10.1(8) GPa				
T(Al)	0.0682(3)	0.1667(1)	0.2022(5)	0.0071(7)
Ca	0	0.5	0	0.0125(7)
M1(Mg, 11.95 e^-)	0	0	0.5	0.006(1)
M2(Mg, 12.12 e^-)	0	0.3306(2)	0.5	0.005(1)
O1	-0.0789(12)	0	0.1398(19)	0.016(1)
O2	0.3593(9)	0.1873(4)	0.1392(13)	0.0164(9)
O3	0.1296(8)	0.1678(3)	0.3834(13)	0.013(1)
OH	0.1264(11)	0.5	0.3901(18)	0.015(1)

Table 3. Bond distances (Å), polyhedral volumes (Å^2), ditrigonal distortion angle (α, °) and interlayer thickness (*I*, Å) at different pressures.

P (GPa)	0.0001*	0.60(8)	1.80(8)	3.31(8)	4.84(8)	6.25(8)	7.80(8)	10.1(8)
Ca-O1 x 2	2.455(6)	2.450(5)	2.432(6)	2.410(8)	2.381(8)	2.361(5)	2.347(9)	2.311(10)
Ca-O2 x 4	2.452(5)	2.446(4)	2.420(5)	2.402(7)	2.374(7)	2.360(4)	2.340(7)	2.309(9)
<Ca-O>	2.453	2.447	2.424	2.405	2.376	2.360	2.342	2.310
V(Ca)	19.64(6)	19.49(5)	18.94(7)	18.52(9)	17.89(9)	17.53(5)	17.13(9)	16.4(1)
M1-OH x 2	2.036(5)	2.024(4)	2.006(6)	2.015(7)	2.020(7)	2.007(4)	2.003(8)	2.001(9)
M1-O3 x 4	2.079(5)	2.061(4)	2.056(5)	2.058(8)	2.048(7)	2.041(4)	2.036(7)	2.029(8)
<M1-O>	2.065	2.049	2.039	2.044	2.039	2.030	2.025	2.020
V(M1)	11.61(5)	11.29(4)	11.04(6)	11.24(8)	11.15(7)	11.00(4)	10.94(7)	10.84(8)
M2-O3 x 2	2.031(4)	2.015(3)	2.012(4)	2.017(7)	2.013(6)	2.003(4)	2.000(6)	1.998(7)
M2-O3' x 2	2.057(4)	2.040(3)	2.029(5)	2.036(7)	2.028(6)	2.021(4)	2.018(6)	2.010(7)
M2-OH x 2	2.037(5)	2.022(4)	2.006(5)	2.018(7)	2.013(7)	2.002(4)	1.999(7)	1.996(9)
<M2-O>	2.042	2.026	2.016	2.024	2.018	2.009	2.006	2.001
V(M2)	11.24(5)	10.94(4)	10.69(5)	10.93(8)	10.84(7)	10.69(4)	10.64(7)	10.56(9)
T-O1	1.729(3)	1.727(3)	1.721(4)	1.717(5)	1.713(5)	1.716(3)	1.712(5)	1.713(6)
T-O2	1.728(4)	1.725(4)	1.724(5)	1.717(6)	1.713(6)	1.716(3)	1.710(6)	1.710(8)
T-O2'	1.727(3)	1.725(3)	1.724(4)	1.718(4)	1.718(4)	1.714(3)	1.717(5)	1.715(6)
T-O3	1.716(8)	1.726(6)	1.713(8)	1.692(14)	1.696(11)	1.678(7)	1.671(12)	1.672(14)
<T-O>	1.725	1.725	1.721	1.711	1.710	1.706	1.703	1.702
V(T)	2.63(2)	2.64(1)	2.62(2)	2.57(3)	2.56(2)	2.54(1)	2.53(2)	2.53(3)
α	23.00(4)	23.08(3)	23.17(4)	23.37(5)	23.32(5)	23.71(3)	23.79(6)	23.50(8)
I	3.10(2)	3.10(2)	3.04(2)	3.01(3)	2.92(3)	2.92(2)	2.89(3)	2.74(4)

Note: $\alpha = 1/6 \cdot \sum_{i=1}^{6} \left| 120° - \varphi_i \right| /2$, where φ_i is the angle between basal edge of neighbouring tetrahedra articulated in the 6mR (Brigatti and Guggenheim 2002). Polyhedral volumes calculated using the software IVTON (Balic-Zunic and Vickovic 1996) .

Table 4 (Deposited) Unit-cell parameter of clintonite at high temperature.